Oxygen-vacancy-induced ferromagnetism in undoped SnO_2 thin films

G. S. Chang,[1,*] J. Forrest,[1] E. Z. Kurmaev,[2] A. N. Morozovska,[3] M. D. Glinchuk,[3] J. A. McLeod,[1] A. Moewes,[1] T. P. Surkova,[2] and Nguyen Hoa Hong[4]

[1]*Department of Physics and Engineering Physics, University of Saskatchewan, 116 Science Place, Saskatoon, SK, S7N 5E2, Canada*

[2]*Institute of Metal Physics, Russian Academy of Sciences-Ural Division, 620041 Yekaterinburg, Russia*

[3]*Institute of Problems of Material Sciences, National Academy of Sciences of Ukraine, 03028 Kiev, Ukraine*

[4]*Department of Physics and Astronomy, Seoul National University, 599 Gwanak-ro, Gwanak-gu, Seoul 151-747, South Korea*

(Received 27 January 2012; published 25 April 2012)

We investigated the possible formation and segregation of oxygen vacancies near the surface of SnO_2 thin films from oxygen K-edge x-ray emission and absorption spectra and found that the distribution of O $2p$ unoccupied states for ferromagnetic SnO_2 thin films is different from that of postannealed SnO_2 films under oxygen atmosphere showing diamagnetic behavior. This spectroscopic result suggests that oxygen vacancies can be the source of the surface-induced magnetism in SnO_2 thin films. This possibility was then explored by calculating the lowest energy levels of the structural defects (impurities or neutral vacancies) with two localized carriers near the surface of SnO_2 film using a quantum-mechanical approach combined with the image charge method. A magnetic triplet state is found to be the ground state of those defects in the vicinity of the SnO_2 surface, whereas the nonmagnetic singlet is the ground state of bulk SnO_2. Surface-induced ferromagnetic order can appear at room temperature via 2D magnetic percolation once the vacancy concentration is greater than 3×10^{16} m^{-2}.

DOI: 10.1103/PhysRevB.85.165319 PACS number(s): 75.70.Ak, 71.55.Ht, 78.70.En

I. INTRODUCTION

Oxide-based diluted magnetic semiconductors (DMSOs) have been studied extensively in the last years because of the possibility of controlling both spin and charge of electrons simultaneously in future spintronic devices. Generally, oxide semiconductors having a wide band gap are optically transparent for visible light and thus important for the development of spin-dependent optoelectronics. It is commonly accepted that doping a transition metal plays a key role in inducing ferromagnetism (FM) in these DMS systems.[1–3] However, room temperature FM also has been observed in undoped semiconducting and insulating oxide thin films or nanoparticles, such as HfO_2,[4] In_2O_3,[5,6] TiO_2,[5,7,8] ZnO,[8,9] MoO_2,[10] and SnO_2.[5,11,12] Because these materials in bulk phase are diamagnetic, the origin of FM in these pristine oxide thin films is rather controversial. According to a systematic study of magnetic behaviors of TiO_2, HfO_2, and In_2O_3 thin films grown by pulsed laser deposition (PLD),[6] postannealing of ferromagnetic samples under oxygen atmosphere results in the significant suppression of their magnetic properties. The samples even showed a transition from ferromagnetic to diamagnetic when increasing the postannealing duration up to 8–10 hours. These findings suggested that FM in these undoped oxides might originate from oxygen vacancies (V_O) because postannealing under oxygen atmosphere fills up vacancies.

Meanwhile, theoretical calculations of magnetic oxide thin films have given inconsistent results, especially for SnO_2. Rahman *et al.*[13] found from their density functional theory (DFT) calculations that a Sn vacancy (V_{Sn}) has a magnetic ground state with a large magnetic moment. This indicates that V_{Sn} can be responsible for ferromagnetic ordering, whereas V_O does not induce any magnetism. The problem is that V_{Sn} are unlikely to be formed in SnO_2 because of their high formation energy according to the first-principles calculations of Kilic and Zunger.[14] Calculations by Wang *et al.*[15] suggested that the positively charged monovalent O vacancies (V_O^+) can induce local magnetic moments in bulk SnO_2, and the magnetic coupling between two V_O^+ vacancies is ferromagnetic. However, it has not been clearly explained yet why ferromagnetic behaviors are observed in the thin films of SnO_2 but not in the bulk samples.

In the present paper, we used a quantum mechanical approach combined with the image charge method[16,17] to investigate surface-induced magnetism in SnO_2 thin films as well as the role of oxygen vacancies in inducing ferromagnetic ordering. The spectroscopic results of synchrotron-excited oxygen x-ray emission and absorption spectroscopy for ferromagnetic and diamagnetic SnO_2 thin films also will be discussed.

II. EXPERIMENTAL

The 220- and 10-nm-thick SnO_2 thin films were grown on $LaAlO_3$(001) substrates using a PLD technique (KrF laser with $\lambda = 248$ nm). Preparation conditions were described elsewhere.[11] The magnetic hysteresis loops were measured at room temperature under magnetic fields up to 0.5 T using a superconducting quantum interference device (Quantum Design Inc.).

Oxygen K-edge x-ray emission spectroscopy (XES) and x-ray absorption spectroscopy (XAS) measurements were performed at Beamline 8.0.1 of the Advanced Light Source at Lawrence Berkeley National Laboratory.[18] The endstation uses a Rowland circle geometry x-ray spectrometer equipped with spherical gratings. For the O $K\alpha$ XES spectra, the samples were excited near the O $1s$ ionization threshold (excitation energy, $E_{exc} = 540.8$ eV) to suppress the high-energy satellite structure. The O $1s$ XAS spectra were acquired in the surface-sensitive total electron yield mode, and the oxygen XAS measurements of bulk SnO_2 were acquired using a channel

plate fluorescence detector to measure the bulk sensitive total fluorescence yield. The spectral energies of O K-edge XES and XAS spectra were calibrated using the emission (526.0 eV) and absorption (532.7 eV) peaks of a bismuth germanium oxide reference,[19] and the intensity was normalized to the incident photon current using a highly transparent gold mesh in front of the sample to measure the intensity fluctuations in the photon beam. To estimate the band gap of these materials in a consistent manner, we made use of peaks in the second derivative of the XAS and XES spectra. Using local maxima in the second derivative has been shown to be a good tool for estimating the band gap in oxides.[20,21]

III. CALCULATIONAL DETAILS

The magnetic parameters are calculated by the direct variational method used to solve the Schrödinger–Vanjie equation in the effective mass approximation, allowing for the defect-carrier Coulomb interaction, along with the image charge contribution near the ideal flat surface.[16] The local electronic center approach, as proposed by Deigen *et al.*,[17] was also used to find the ground state of the one-electron impurity center located near the flat surface. We calculated the lowest energy levels of the impurities and neutral vacancies with two carriers (electrons or holes) localized at point $\mathbf{r}_0 = (0, 0, z_0)$ near the surface ($z = 0$) of the SnO_2 film (see Fig. 1).

The image charge method is based on the continuous medium approach, which requires the conception of a media dielectric permittivity (ε) to describe the Coulomb potential induced by a charged defect. The potential is grounded when the characteristic size of the carrier localization (r_d) at the defect center is several times larger than the lattice constant.[22–24] When the defects are immobile, the static dielectric permittivity should be used. Therefore, the polaronic

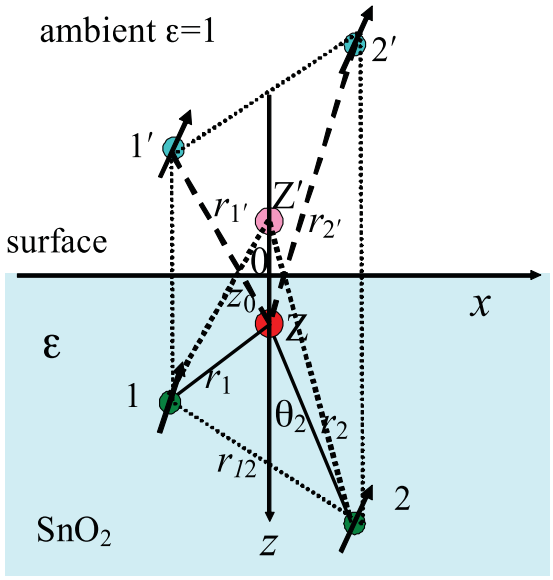

FIG. 1. (Color online) Defect at distance z_0 under the SnO_2 film surface. Two carriers (electrons or holes) 1 and 2 (shown by green circles with arrows) are localized near the defect with effective charge Ze (shown by red [dark gray] circle). Carrier image charges are shown as 1′ and 2′, defect image is Z′.

effects and dielectric anisotropy are neglected in our calculations, i.e., we used the effective static permittivity $\varepsilon = \sqrt{\varepsilon_\perp \varepsilon_{||}}$, which is about 11.75 for SnO_2 with $\varepsilon_{||} = 9.86$ and $\varepsilon_\perp = 14.0$.[25]

In the continuum media approach, cation or anion vacancies are considered the defects placed in a perfect host lattice. We assume neutral vacancies or defects with valency $\pm 2e$, which capture two carriers (electrons or holes), e.g., a F^0 center. For the case of the cation vacancy, a cation atom is added to form the perfect host lattice, and its two electrons are localized at the nearest anions. As a result, a negatively charged defect $(-2e)$ with two holes appears in the continuous media. The situation is reversed for an anion vacancy: it can be modeled as a positively charged defect $(+2e)$ with two electrons in the continuous media.

Note that the effective mass approximation typically describes p-states much better than s-states because the inequality $r_d \gg a$ (where $a = 4.74$ Å and $c = 3.19$ Å are the SnO_2 lattice parameters) is necessary for a valid approximation of the carriers' wave-functions for the s-states. For the p-states that are zero at the defect site, the corresponding wave functions are not sensitive to the concrete short-range peculiarities of the defect potential.[26] That is why, in the calculations of the energy levels of the surface defects constructed from $2p_z$ and $3p_z$ states, we used the effective mass value $\mu = \sqrt{\mu_\perp \mu_{||}} = (0.259 \pm 0.005) m_e$ estimated from the bulk SnO_2 effective mass tensor $\mu_{||} = 0.234 m_e$ and $\mu_\perp = (0.287 \pm 0.012) m_e$ (m_e is the mass of a free electron) obtained by DFT in Ref. 27.

The coordinate dependence of one-fermion (electron or hole) wave functions is chosen in the eigenfunction form of the hydrogen-like atom localized at defect site $r_0 = (0,0,z_0)$,

$$\varphi_{nlm}(\mathbf{r}) \sim R_{nl}\left(\alpha\,|\mathbf{r} - \mathbf{r}_0|\right) Y_{lm}(\theta,\phi) \qquad (1)$$

where $R_{nl}(r)$ are the radial functions, $Y_{lm}(\theta,\phi)$ are spherical harmonics, and $z = r\cos\theta$. The variational parameters (e.g., α) can be determined from the energy minimum in the first order of conventional perturbation theory where the carrier-carrier Coulomb interaction and all interactions with the image charges are considered perturbations.

The wave functions for the carriers localized near a surface defect should be almost zero in vacuum or ambient atmosphere because of the high energy barrier determined by the work function at the solid/ambient interface. Therefore, we select the trial functions satisfying the boundary condition, $\varphi_{nlm}(x,y,z = 0) = 0$. This condition corresponds to the infinitely high barrier at the boundary between the solid and ambient medium (e.g., vacuum, atmosphere, or dielectric soft matter). In the case that the defect is located at the surface (i.e., $z_0 = 0$), the lowest wave function satisfying the boundary condition is the $2p_z$ state:

$$\varphi_{210}(\mathbf{r}) = A(\alpha, z_0) z \exp\left(-\alpha\,|\mathbf{r} - \mathbf{r}_0|\right), \qquad (2)$$

where α is the variational parameter and $A(\alpha,z_0)$ is the normalization constant. The next excited state is the $3p_z$ state:

$$\varphi_{310}(\mathbf{r}) = B(\beta,z_0) z [b(z_0) - \beta|\mathbf{r} - \mathbf{r}_0|] \exp(-\beta|\mathbf{r} - \mathbf{r}_0|), \qquad (3)$$

where β is a variational parameter, $B(\beta,z_0)$ is the normalization constant, and b is a variational parameter with $b = 2$ for the surface defect at $z_0 = 0$. As anticipated for the lowest states

of the hydrogen-like atoms in the bulk, these trial $2p_z$ and $3p_z$ wave functions should be transformed into the spherically symmetric $1s$ and $2s$ functions correspondingly in the limit $z_0 \to \infty$. The condition can be achieved by the transition of $b(z_0 \to \infty) \to 1$.

The two-fermion coordinate wave functions can be constructed from the functions $\varphi_{210}(\mathbf{r})$ and $\varphi_{310}(\mathbf{r})$ in the unique way:

$$\text{Singlets:} \quad \Psi_{22}(\mathbf{r}_1,\mathbf{r}_2) = \varphi_{210}(\mathbf{r}_1)\varphi_{210}(\mathbf{r}_2), \tag{4}$$

$$\Psi^S_{23}(\mathbf{r}_1,\mathbf{r}_2) = \frac{1}{\sqrt{2}}\left[\phi_{210}(\mathbf{r}_1)\phi_{310}(\mathbf{r}_2) + \phi_{210}(\mathbf{r}_2)\phi_{310}(\mathbf{r}_1)\right], \tag{5}$$

$$\Psi_{33}(\mathbf{r}_1,\mathbf{r}_2) = \varphi_{310}(\mathbf{r}_1)\varphi_{310}(\mathbf{r}_2), \quad \text{and} \tag{6}$$

$$\text{Triplet:} \quad \Psi^T_{23}(\mathbf{r}_1,\mathbf{r}_2) = \frac{1}{\sqrt{2}}[\phi_{210}(\mathbf{r}_1)\phi_{310}(\mathbf{r}_2) - \phi_{210}(\mathbf{r}_2)\phi_{310}(\mathbf{r}_1)], \tag{7}$$

with the full spin of zero for singlets ($S = 0$) and one for triplets ($S = 1$).

The energy levels are now calculated within the framework of conventional perturbation theory as $E_{mn} = \langle \Psi_{mn} | \hat{H} | \Psi_{mn} \rangle$. The magnetic triplet state E^T_{23} appears to be the ground state of the impurities and neutral vacancies in the vicinity of the SnO_2 surface, whereas the nonmagnetic singlet E_{22} is the ground state in the bulk. The energy difference between the lowest triplet and singlet states strongly depends on the carrier effective mass μ, dielectric permittivity of the film ε, and distance from the surface z_0. The triplet state E^T_{23} should become the magnetic one ($S_z = \pm 1$), allowing for Hund's rule to orient two fermion (electron or hole) spins in the same direction. This situation will lead to surface-induced magnetism in SnO_2 in the case of the appearance of long-range ferromagnetic order, as will be estimated below.

We note that the pair exchange energy $J_{23}(r)$ of the identical surface defects in SnO_2 (two vacancies or impurity atoms with four shared electrons or holes) reveals a ferromagnetic spin state (i.e., $J_{23}(r) > 0$) independent of the distance r between the defects, but the exchange integral value is significant at distances $R \sim 2 - 10a^*_B$ and has a pronounced maximum at distances $R \sim 5a^*_B$, where $a^*_B = (1+\varepsilon)\pi\varepsilon_0\hbar^2/\mu e^2$ is the effective Bohr radius.

IV. RESULTS AND DISCUSSION

A. Magnetic behaviors of SnO_2 thin films

Figure 2 shows the magnetic hysteresis loops of as-grown and postannealed SnO_2 thin films taken at 300 K. Both 10- and 220-nm-thick as-grown SnO_2 thin films are found to show a strong ferromagnetic signal, whereas the 220-nm film becomes diamagnetic after postannealing in an oxygen atmosphere. This suggests that the presence of oxygen vacancies in as-grown samples is responsible for the ferromagnetic ordering in SnO_2 films because those vacancies are expected to be filled up upon postannealing. On the other hand, an interesting result is the thickness dependence: the 220-nm-thick SnO_2 film has a saturated magnetization that is much smaller than that of the 10-nm-thick film. If the supposition of oxygen vacancies responsible for FM in SnO_2 is correct, this result might suggest that the oxygen vacancies would be located mostly at the surface (to air) and/or the interface (between film and substrate), but much less in deeper layers.[11]

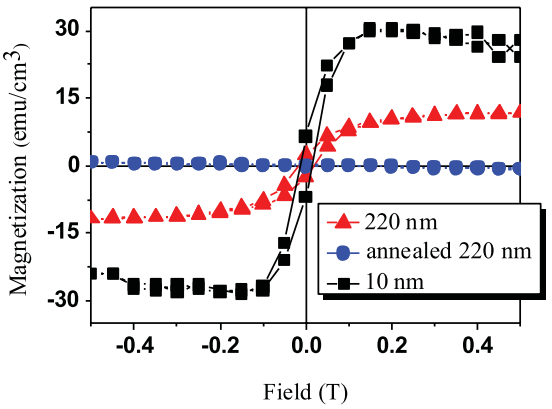

FIG. 2. (Color online) Magnetization versus magnetic field taken at 300 K as the magnetic field is applied parallel to the film's plane for the as-grown 10-nm-thick SnO_2 film, the as-deposited 220-nm-thick SnO_2 film, and the 220-nm-thick SnO_2 film postannealed under the O_2 atmosphere of 760 Torr at 700 °C for 10 hours.

B. Theoretical estimations of the surface-induced ferromagnetism in SnO_2

We turn our attention now to discuss semi-quantitatively the possible mechanisms for the appearance of long-range ferromagnetic order between the structural defects (vacancies) near the surface region. The defect-induced FM can have a percolative nature,[28] especially in thin films, when the dimensionality of the system is reduced to 2D by the spatial confinement. For the continuous media approximation used in our calculations, the most appropriate is the well-known percolation problem of circles, with random magnetic defects placed in the center of a circle[24] The number of overlapping circles is equal to the average number of interacting defects inside a circle: $B_{2D} = \pi N_{2D} r_j^2$, where r_j and N_{2D} are the exchange radius and the 2D concentration of the magnetic vacancies, respectively. The critical number of the overlapping circles was calculated to be $B^c_{2D} \approx 4$.[24] Next, the critical percolation concentration (N^c_{2D}) of the random magnetic defects should be determined for a known radius r_j as $N^c_{2D} = 4/\pi r_j^2$. The exchange radius was determined from the condition of the exchange energy being equal to the thermal energy at $J_{23}(r_j) = k_B T_r$, where T_r is room temperature (300 K).

The surface-induced magnetism parameters calculated for SnO_2 thin films are presented in Table I. To summarize the estimations, the surface-induced magnetic states of oxygen vacancies possibly present at the surface of SnO_2 and below the surface. The surface-induced long-range ferromagnetic ordering could originate in SnO_2 at room temperature for vacancy concentrations greater than 1.5×10^{16} m^{-2} to 3×10^{16} m^{-2}. However the energy level differences are about $0.024 \sim 0.032$ eV; thus, both magnetic triplet and nonmagnetic singlet could be occupied at room temperature because the activation energy at room temperature is about 0.025 eV.

TABLE I. The surface-induced magnetism parameters of SnO_2 (permittivity $\varepsilon = 11.75$, $a = 0.474$ nm and $c = 0.319$ nm).

Effective mass, μ	0.2 m_e	0.25 m_e	0.3 m_e
Effective Bohr radius, a_B^*	0.85 nm	0.71 nm	0.56 nm
Carrier localization radius r_d for φ_{210}	1.91 nm	1.59 nm	1.27 nm
Carrier localization radius r_d for φ_{310}	3.41 nm	2.85 nm	2.28 nm
Lowest triplet E_{23}^T	− 0.0635 eV	− 0.0794 eV	− 0.0952 eV
Lowest singlet E_{23}^S	− 0.0613 eV	− 0.0766 eV	− 0.0920 eV
Energy difference $(E_{23}^S - E_{23}^T)$	0.022 eV	0.028 eV	0.032 eV
Depth z_0 when $E_{23}^T < E_{22}$	1.7 nm	1.4 nm	1.1 nm
Exchange radius, r_j	$11a_B^* \approx 9.3$ nm	$12a_B^* \approx 8.5$ nm	$13a_B^* \approx 7.3$ nm
Critical percolation concentration, N_{2D}^c	1.47×10^{16} m^{-2}	1.76×10^{16} m^{-2}	2.39×10^{16} m^{-2}

C. Oxygen *K*-edge x-ray emission and absorption spectra of SnO_2 thin films

According to the magnetic measurements (Fig. 2) and calculated surface-induced magnetism parameters (Table I), one can suppose that oxygen vacancies created near the surface can induce FM in very thin pristine SnO_2 films. To verify this, we have measured oxygen *K*-edge x-ray emission (O $K\alpha$ XES) and absorption (O 1*s* XAS) spectra, which probe the distribution of occupied and unoccupied O 2*p* densities of state, respectively.

Figure 3 shows that the fine structure of the O $K\alpha$ XES and O 1*s* XAS for 10-nm SnO_2 thin film is different with respect to those of the as-grown and postannealed 220-nm SnO_2 films: the B-C fine structure of O $K\alpha$ XES is smeared, and the main features a and d in O 1*s* XAS are shifted to higher energy by about 1.5 eV. The origin of these peaks is clear from our electronic structure calculations as displayed in Fig. 4. Feature A of O $K\alpha$ XES spectra mainly originates from occupied O 2*p* states with small admixture of Sn *d* states, whereas peaks B and C are due to hybridized O

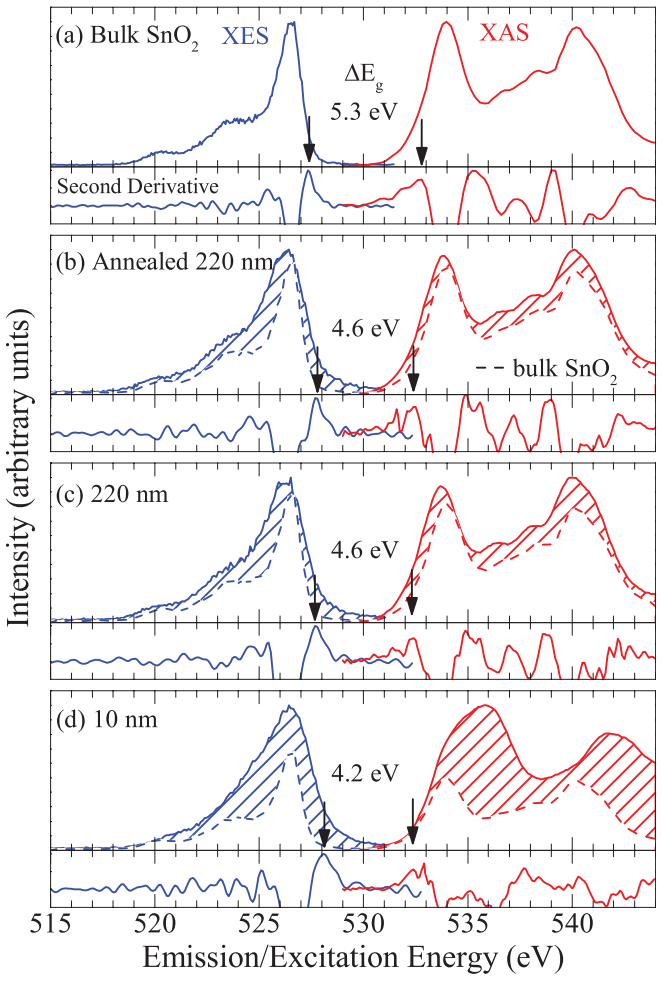

FIG. 3. (Color online) O *K*-edge x-ray emission (O $K\alpha$ XES) and absorption (O 1*s* XAS) spectra for bulk SnO_2 (a), the 200-nm-thick SnO_2 thin film with postannealing treatment (b), the 200-nm-thick as-grown film (c), and the 10-nm-thick as-grown film.

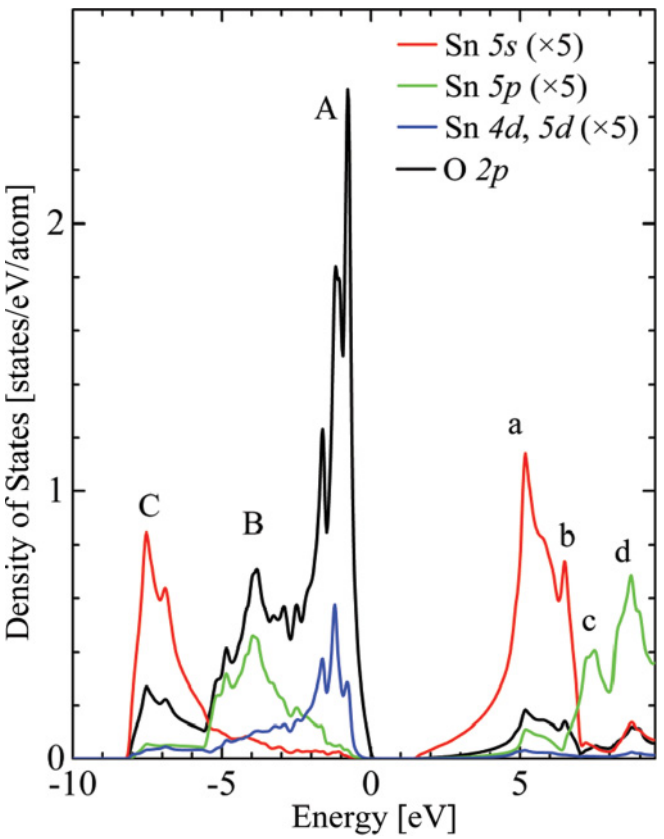

FIG. 4. (Color online) Calculated partial densities of states for bulk SnO_2.

$2p$-Sn $5p$ and O $2p$-Sn $5s$ states, respectively. Features a-b and c-d of the O $1s$ XAS spectra are caused by strongly hybridized O $2p$-Sn $5s$ and O $2p$-Sn $5p$ vacant states, respectively.

The smearing of B-C spectral features of the O $K\alpha$ XES spectrum of 10-nm SnO_2 thin film, as shown in Fig. 3, can be explained by a disordering effect induced by oxygen vacancies, which also can lead to the redistribution of the O $2p$ vacant states seen in O $1s$ XAS spectra. It is well known that the presence of oxygen vacancies can lead to a reduction of band gap in binary oxides. This means one can expect the reduction of band gap for an oxygen-deficient SnO_2 thin film. The combination of oxygen x-ray K-emission and absorption spectra allows one to make such estimations (see Refs. 21 and 22 for details). According to these estimates and spectral features in Fig. 3, the band gap is reduced from 4.6 eV for postannealed diamagnetic 220-nm SnO_2 film to 4.2 eV for ferromagnetic 10-nm SnO_2 thin film, where the presence of a significant number of oxygen vacancies was supposed. Therefore, our experimental findings confirm the existence of oxygen vacancies near the surface for 10-nm SnO_2 thin film, which can induce FM.

V. CONCLUSIONS

By combining the data from soft x-ray emission/absorption spectroscopy measurements and the quantum-mechanical approach with the image charge method, we have shown that the observed ferromagnetism in very thin pristine SnO_2 films can be induced by the presence of oxygen vacancies located near the film surface. This behavior should be strongly weakened in thicker films, where the contribution of oxygen vacancies to the volume of sample is much smaller, and it completely disappears for postannealed SnO_2 films under oxygen atmosphere.

ACKNOWLEDGMENTS

We gratefully acknowledge support from the Natural Sciences and Engineering Research Council of Canada (NSERC), the Canada Foundation for Innovation (CFI), and the Canada Research Chair Program. This work was supported by the Seoul National University Foundation Research and by the Russian Foundation for Basic Research (Grant 11-02-00022). A.N.M. gratefully acknowledges E. A. Eliseev for giving valuable advice and NAS of Ukraine for financial support.

*gapsoo.chang@usask.ca

[1] N. H. Hong, J. Sakai, W. Prellier, A. Hassini, A. Ruyter, and F. Gervais, Phys. Rev. B **70**, 195204 (2004).
[2] K. Ueda, H. Tabata, and T. Kawai, Appl. Phys. Lett. **79**, 988 (2001).
[3] M. Venkatesan, C. B. Fitzgerald, J. G. Lunney, and J. M. D. Coey, Phys. Rev. Lett. **93**, 177206 (2004).
[4] M. Venkatesan, C. B. Fitzgerald, and J. M. D. Coey, Nature **430**, 630 (2004).
[5] A. Sundaresan, R. Bhargavi, N. Rangarajan, U. Siddesh, and C. N. R. Rao, Phys. Rev. B **74**, 161306(R) (2006).
[6] N. H. Hong, J. Sakai, N. Poirot, and V. Brize, Phys. Rev. B **73**, 132404 (2006).
[7] S. D. Yoon, Y. Chen, A. Yang, T. L. Goodrich, X. Zuo, D. A. Arena, K. Ziemer, C. Vittoria, and V. G. Harris, J. Phys.: Condens. Matter **18**, L355 (2006).
[8] N. H. Hong, J. Sakai, and V. Brizé, J. Phys.: Condens. Matter **19**, 036219 (2007).
[9] Q. Xu, H. Schmidt, S. Zhou, K. Potzger, M. Helm, H. Hochmuth, M. Lorenz, A. Setzer, P. Esquinazi, C. Meinecke, and M. Grundmann, Appl. Phys. Lett. **92**, 082508 (2008).
[10] P. Thakur, J. C. Cezar, N. B. Brookes, R. J. Choudhary, R. Prakash, D. M. Phase, K. H. Chae, and R. Kumar, Appl. Phys. Lett. **94**, 062501 (2009).
[11] N. H. Hong, N. Poirot, and J. Sakai, Phys. Rev. B **77**, 033205 (2008).
[12] C. E. Rodríguez Torres, L. Errico, F. Golmar, A. M. Mudarra Navarro, A. F. Cabrera, S. Duhalde, F. H. Sánchez, and M. Weissmann, J. Magn. Magn. Mater. **316**, e219 (2007).
[13] G. Rahman, V. M. García-Suárez, and S. C. Hong, Phys. Rev. B **78**, 184404 (2008).
[14] Ç. Kılıç and A. Zunger, Phys. Rev. Lett. **88**, 095501 (2002).
[15] H. Wang, Y. Yan, K. Li, X. Du, Z. Lan, and H. Jin, Phys. Stat. Sol. (b) **247**, 444 (2010).
[16] A. N. Morozovska, E. A. Eliseev, M. D. Glinchuk, and R. Blinc, Physica B **406**, 1673 (2010).
[17] M. F. Deigen and M. D. Glinchuk, Surf. Sci. **3**, 243 (1965).
[18] J. J. Jia, T. A. Callcott, J. Yurkas, A. W. Ellis, F. J. Himpsel, M. G. Samant, J. Stöhr, D. L. Ederer, J. A. Carlisle, E. A. Hudson, L. J. Terminello, D. K. Shuh, and R. C. C. Perera, Rev. Sci. Instrum. **66**, 1394 (1995).
[19] N. W. Johnson, J. A. McLeod, and A. Moewes, J. Phys.: Condens. Matter **23**, 445501 (2011).
[20] E. Z. Kurmaev, R. G. Wilks, A. Moewes, L. D. Finkelstein, S. N. Shamin, and J. Kunes, Phys. Rev. B **77**, 165127 (2008).
[21] J. A. McLeod, R. G. Wilks, N. A. Skorikov, L. D. Finkelstein, M. Abu-Samak, E. Z. Kurmaev, and A. Moewes, Phys. Rev. B **81**, 245123 (2010).
[22] I. E. Tamm, Sow. Phys. **1**, 733 (1932).
[23] L. D. Landau, E. M. Lifshitz, and L. P. Pitaevskii, *Electrodynamics of Continuous Media*, 2nd ed. (Butterworth-Heinemann, Oxford, 1984).
[24] B. I. Shklovski and A. L. Efros, *Electronic properties of doped semiconductors* (Springer-Verlag, Berlin, New York, 1984).
[25] D. M. Roessler and W. A. Albers, J. Phys. Chem. Soc. **33**, 293 (1972).
[26] A. I. Anselm, *Introduction to Semiconductor Theory* (Mir, Moscow/Prentice-Hall, Englewood Cliffs, NJ, 1981).
[27] K. J. Button, C. G. Fonstad, and W. Dreybrodt, Phys. Rev. B **4**, 4539 (1971).
[28] J. Hu, Z. Zhang, M. Zhao, H. Qin, and M. Jiang, Appl. Phys. Lett. **93**, 192503 (2008).